*Clay Minerals*, (2017) **52**, 329–340

# Properties and characterization of a clay raw material from Miličinica (Serbia) for use in the ceramic industry

MAJA MILOŠEVIĆ* AND MIHOVIL LOGAR

*Faculty of Mining and Geology, University of Belgrade, Đušina 7, 11000 Belgrade, Serbia*

(*Received 20 April 2017; revised 15 September 2017; Associate Editor: Joao Labrincha*)

ABSTRACT: The present study focused on the assessment and possible applications of the clay from the Miličinica deposit, western Serbia. X-ray diffraction (XRD), Infrared (IR) spectroscopy, Inductively Coupled Plasma Optical Emission Spectrometry (ICP-OES), Differential Thermal Analysis and Thermogravimetry (DTA-TG) and High Temperature Microscopy (HTM) were used to characterize the clay in question. The physical properties determined were colour, plasticity, specific surface area, particle-size distribution and cation exchange capacity (CEC). Clay minerals are the main phases in the samples studied, with illite being the predominant phase and kaolinite being present in variable amounts. Quartz, feldspars, carbonates and iron-bearing minerals were also detected. Varied technological behaviours were expected because of the mineralogy (illite and iron contents), average grain size (0.6–0.7 μm), specific surface area (≈60 $m^2$/g) and plasticity index (≈13%). The classification of the clays studied, based on the main characteristics and using appropriate diagrams, suggests that they are easily adaptable for ceramic processes.

KEYWORDS: clay, raw material, kaolinite, illite, ceramic industry.

Clays are among the most important raw materials used in the fabrication of ceramic products (Norton, 1970; Burst, 1991; Vieira *et al.*, 2008; Kamseu *et al.*, 2007). Minerals of the kaolin group play a significant role in the ceramic industry (Prasad *et al.*, 1991; Murray, 1991, 1995; Murray & Kogel, 2005; Mukherjee, 2013) but they also find application as fillers in paint or paper (Bundy & Ishley, 1991; Murray & Kogel, 2005), cosmetics (Silva-Valenzuela *et al.*, 2013; Valášková, 2015), in pharmaceuticals (Viseras *et al.*, 2007; Carretero & Pozo, 2009), *etc*. The most important ceramic product is porcelain. Porcelain is usually composed of two main types of components: plastic and non-plastic. The plastic components are clay minerals (usually of the kaolin group) and the non-plastic ones are inert minerals (*e.g.* quartz), fluxes (*e.g.* feldspars) and flux-inducing minerals (*e.g.* carbonates) (Matthew & Fatile, 2014). Similar raw materials have been named either "kaolin" or "ball clay" depending on their end use (Harvey & Murray, 1997; Dondi *et al.*, 2014). According to the definition: "Ball clay is a fine-grained, highly plastic, mainly kaolinitic sedimentary clay, the higher grades of which fire to a white or near white colour" (Wilson, 1998; Dondi *et al.*, 2014). Kaolins are deeply altered parent rocks that contain abundant non-plastic components with at least 40% <2 μm particles, while kaolinitic loams represent sedimentary deposits with kaolinite in admixture with larger amounts of quartz and other clay minerals such as illite, smectite, interstratified illite-smectite, *etc*. (Dondi *et al.*, 2014). The impurities present in the raw material, such as iron minerals, carbonate minerals, quartz, feldspar, pyrite, *etc*. (Grimshaw, 1971) affect the main characteristics and therefore affect its

* E-mail: maja.milosevic@rgf.bg.ac.rs
https://doi.org/10.1180/claymin.2017.052.3.04

utilization (Saikia *et al.*, 2003). The use of clay in commercial manufacture of different types of tiles depends on the technological and appearance requirements, namely the firing colour after and the behaviour during manufacturing (Dondi *et al.*, 2014). Due to complex mineralogical and chemical compositions and the physical characteristics, clays have unique properties that are characteristic of their deposits (Saikia *et al.*, 2003; Vieira *et al.*, 2008; Mitrović *et al.*, 2009; Boussen *et al.*, 2016, among others). Based on their mineralogical, chemical, granulometric and rheological characteristics, a realistic assessment of the potential industrial application of the raw materials is feasible (Dondi *et al.*, 2014).

Kaolins have been investigated in few locations in W. Serbia (Radosavljević *et al.*, 1994, 2014). Miličinica, in the Valjevo district, is endowed with a large clay deposit which has not yet been exploited fully. According to the 'Kaolin', a.d. Valjevo, Serbia, a mining company with a history of >50 years, the annual production is ~70,000 t with a possibility to expand to fulfill industrial needs. Few papers have reported mineral characteristics of this deposit and the data available in the literature are incomplete in terms of physical properties (*e.g.* Mitrović *et al.*, 2009; Milošević *et al.*, 2016). The 'Miličinica' deposit is associated with kaolinite clay that has a larger amount of iron-bearing minerals, which limit its utility, but contains a favourable amount of illite which imparts properties useful in some ceramic industries. Due to the geographic position of the deposit and its short distance from the tile factories it presents a good source of raw kaolin at low cost. The major ceramic industries in Serbia use clay from this deposit on a daily basis. Systematic investigation of the characterization of the clay is needed to reach maximum potential.

The objective of the present work was to characterize the clays found in a deposit of Miličinica in the municipal area of Valjevo, Serbia, to promote exploitation of raw materials for production of building ceramics.

## *Location and geological setting*

The Miličinica deposit is situated ~90 km SW of Belgrade (Fig. 1, left, marked with a black triangle), at the edge of the Pannonian basin. Pannonian sediments are represented by marls, clays, quartz sands and gravels, developed over a wide area in the Posavo-Tamnava and Pocerina region of Serbia (Fig. 1, right). The largest area with these sediments is near the Višnjica and Mlakve rivers. The deposits in Miličinica region are characterized by high-quality quartz sands and kaolinitic clays.

The clays occur at different levels of the Miocene series and show gradual transition from plastic to sandy clay and quartz sands. They form lenses of various sizes and variable thickness (1–15 m) and lie at a relatively shallow depth, 2–35 m (Filipović *et al.*,

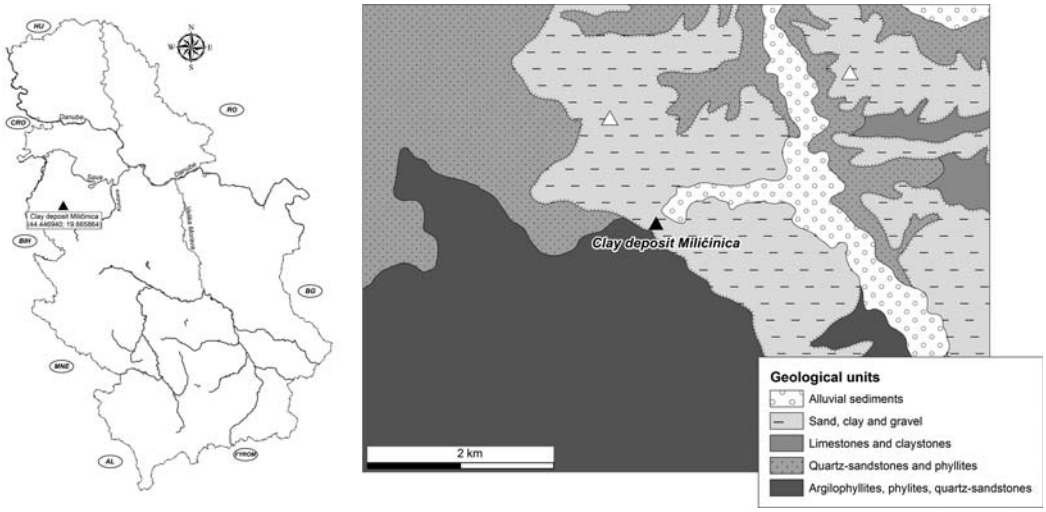


FIG. 1. (left) Location and geological setting of the Miličinica clay deposit, Serbia; (right, black triangle), together with the well known clay deposits (white triangle) (Basic Geological Map of Serbia 1:100,000, Vladimirci sheet).

https://doi.org/10.1180/claymin.2017.052.3.04 Published online by Cambridge University Press

1973; Radosavljević *et al.*, 1994). The occurrence of clay lens-like bodies is due to frequent oscillations of the Mio-Pliocene waters. Fine, dispersed clayey material precipitated by lifting and deepening of the basin forming clay deposits. Some of the clay deposits are located in the Mio-Pliocene sediments along the eastern slopes of the Vlašić mountains (Fig. 1, right, marked with a white triangle). These sediments consist of Upper Palaeozoic phyllites, slates and sandstones. Alteration produced a wide range of ceramic and brick clays along with quartz sands (Filipović *et al.*, 1973; Radosavljević *et al.*, 1994).

## MATERIALS AND METHODS

The clay was collected from exposed faces of the Miličinica deposit with the permission of the governing company Kaolin, a.d. Valjevo, Serbia. The deposit comprises two different layers of clay separated by colour: M1 – white and M2 – yellow. The third sample, M3, represents a mixture of the M1 and M2 clays from different parts of the deposit (1 kg each, prepared by the Kaolin company). The samples were dried at room temperature, crushed and homogenized. The clay fraction (<2 μm) was separated from the bulk clays by sedimentation in distilled water.

The grain-size distribution in suspended raw samples was determined by the pipette method according to the DIN ISO 11277 (2002). Dark-field microscopy (FLUOVAL2 (Carl Zeiss)) was applied for measurements of suspended <2 μm particles. The suspensions were photographed using a Canon, Power Shot (SX 220 HS) camera and were processed using the *ImageJ* program. The specific surface was calculated according to the average particle size.

Powder XRD data were obtained with a Philips PW 1710 diffractometer using Cu-*K*α radiation with a step size of 0.02°2θ and scanning time of 1 s per step. Randomly oriented samples were examined in the intervals 3–60°2θ and oriented samples from 3 to 15° 2θ. The oriented samples were examined as air dried (AD), after solvation with ethylene glycol (EG) and after heating at 450°C (H). Phase identification followed ICSD cards 68698 – kaolinite, 166961 – illite, 18172 – quartz, 40000 – feldspar.

The chemical composition was determined by inductively coupled plasma optical emission spectrometry, using a Thermo Scientific iCAP 6500 Duo ICP-OES spectrometer (Thermo Fisher Scientific, Cambridge, UK), equipped with a RACID86 Charge Injector Device (CID) detector, a pneumatic cross-flow type nebulizer, quartz torch, and alumina injector, which allowed detection of samples containing small amounts of HF. The optical system was purged with argon and the Echelle polychromator thermostated at 38°C. The detection limit for the elements analysed was ~0.1 mg/L.

The cation exchange capacity (CEC) of the samples was determined after saturation with methylene blue (MB) solution according to ASTM C387-99 (1984), using a uniSPEC2 spectrophotometer. Quantitative determination of carbon content was performed by calcimetry according to the AFNOR NF EN ISO 10693 (1995) standard. Infrared spectroscopic analysis was performed using a Perkin Elmer 597 spectrometer with the KBr pellet method in the region 4000–200 $cm^{-1}$.

The colour and whiteness of the raw and pressed powder samples after firing at 1200°C (10°C/min, Hereuse furnace), were established from the diffuse reflectance (DR) spectra using a CCS200 spectrometer (Thorlabs) with R45/45 geometry in the region between 400 and 700 nm according to the CIE (1932) method. The white standard was $BaSO_4$ and the light source was illuminant C. The whiteness (W) was determined from the luminous reflectance (Y),

$$W(\%)Y = \sum_{400}^{700} R_\lambda y_\lambda E_\lambda \Delta_\lambda$$

where $R = R(\text{sample})/R(\text{standard})$, $y$ is the y tristimulus value, $E$ is the energy distribution of illuminant C and $\Delta = 5$ nm.

Differential thermal analysis (DTA) was performed on a modernized A.D.A.M.E.L furnace equipped with a Pt-PtRh thermocouple and BK PRECISION XLN15010 DC power supplies as heating rate controller. All measurements were performed in air atmosphere using $Al_2O_3$ as the reference material, over a temperature range of 20–1000°C and heating rate of 10°C/min. Thermal gravimetric (TG) analysis was carried out using a Setsys, SETARAM Instrument, France, over the temperature range 20–1100°C. The samples were placed in an $Al_2O_3$ pan and heated at a rate of 10°C $min^{-1}$ under air flow (20 $cm^3$ $min^{-1}$).

A high-temperature microscope (HTM) (Carl Zeiss, Jena, Germany) equipped with a video system and a digital camera (Canon PRO-1) was used to determine the intervals of sintering, softening and melting of pressed cube samples (3 mm × 3 mm × 3 mm) over the temperature range 20–1400°C (10°C/min). The temperature of the sample was recorded using a PtPt-Rh thermocouple. The dilatation-contraction curve as a function of temperature was evaluated from the relative change of the surface area of the body being examined,

https://doi.org/10.1180/claymin.2017.052.3.04 Published online by Cambridge University Press

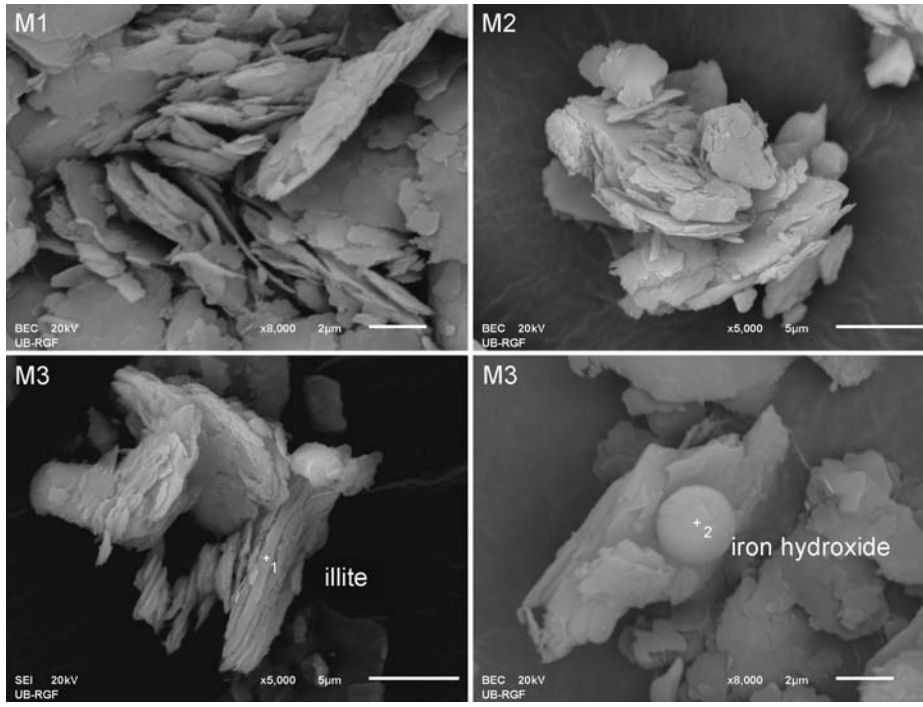


FIG. 2. SEM-BSE and SEI images of pseudo-hexagonal kaolinite stacks and plates with EDXS point of illite and iron oxyhydroxide.

using *ImageJ* software. The 66 images were taken at different temperatures with increasing image frequency around critical points.

Particle morphology and grain-size assessment were determined using Scanning Electron Microscopy (SEM) with a JEOL JSM-6610LV SEM coupled with an Oxford Energy Dispersive X-Max 20 $mm^2$ SDD energy dispersive X-ray spectrometer (EDXS). The analyses were performed with 20 kV acceleration potential and 20 nA beam current using external and internal standards. Calibration of the analysing system was achieved using iron. Samples were coated with gold films (LEICA Model SCD005).

The Atterberg limits were determined according to the Casagrande method (L.C.P.C., 1987). The plastic limit (PL), liquid limit (LL) and plasticity index (PI) were determined according to Atterberg (1911).

## RESULTS AND DISCUSSION

The clay particles display face-to-face associations and their sizes vary between 1 and 5 µm (Fig. 2). Pseudo-hexagonal kaolinite stacks and plates were observed along with less frequent rolled and rough-edged particles. The M1 sample has more regular edge particles while samples M2 and M3 contain flakes mostly with broken edges. Well crystalized, stacked flakes composed of large particles yielded low specific surface area while those with broken edges yielded greater specific surface area and greater adsorption of impurities (Felhi *et al.*, 2008). The rolled particles, present in minor amounts are indicative either of halloysite or of disordered kaolinite (Frost *et al.*, 2002; Joussein *et al.*, 2005). Halloysite may adopt various morphologies according to the crystallization and geological history. Morphology may range from short tubular, spheroidal and platy to elongated tubules which are the most common (Joussein *et al.*, 2005).

TABLE 1. Specific surface area and average grain size of the <2 µm fractions.

| | Samples (<2 µm) | | |
|---|---|---|---|
| | M1 | M2 | M3 |
| Average grain size (µm) | 0.6 | 0.7 | 0.7 |
| Specific surface area ($m^2$/g) | 55.5 | 66.2 | 57.1 |

https://doi.org/10.1180/claymin.2017.052.3.04 Published online by Cambridge University Press

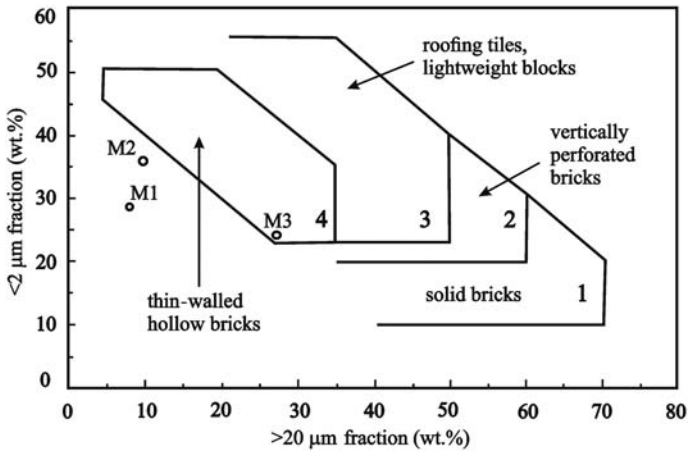


FIG. 3. Technological classification of the clay samples according to Winkler (1954).

Tubular halloysite is commonly derived from feldspars and micas or it may result from alteration of platy kaolinite particles (Singh & Gilkes, 1992; Joussein *et al.*, 2005). Illite (K = 3.20 wt.%) and iron oxyhydroxides (Fe = 54.39 wt.%, O = 42.6 wt.%) were confirmed by EDXS. Illite minerals (Fig. 2) that are precipitated from formation waters in sandstones frequently appear in the form of fibres and laths (Güven, 2001). Iron oxyhydroxides are present in the form of solid spheres.

The grain-size distribution of suspended raw samples is similar in all materials. The <2 μm fraction dominates except for sample M3 where the >20 μm fractions is more abundant (27%). The <2 μm clay fractions of M1, M2 and M3 were 27, 35 and 24% respectively. The average grain size and specific surface area of the 2 μm fractions of the samples were determined by dark field microscopy (Table 1). Particle-size distribution is important in defining the properties of green pastes and suspensions during their drying or firing (Rivi & Ries, 1997; Boussen *et al.*, 2016).

Assessment of the clays based on the average grain size <2 μm and >20 μm only, was performed by means of a Winkler diagram (Fig. 3). The projection indicates suitability for production of vertically perforated bricks (M1 and M2) and hollow products (M3) (Winkler, 1954; Dondi *et al.*, 1998; Boussen *et al.*, 2016).

The clay colour affects the appearance of the finished product. Large percentages of iron oxide or iron-bearing clays tend to produce brown/orange fired clay bodies (Lawrence, 1972; Murray, 2007). The whiteness index (L) represents the degree to which a surface reflects light and has a value of 100% for a pure white colour. The samples have L values ranging from 49.5 to 57.4% before firing (Table 2, left). The M2 and M3 samples absorb more in the blue region compared to sample M1 and have higher yellowness due to its greater $Fe_2O_3$ content.

The amount of iron minerals (goethite >9%) in M2 and M3 might have a significant influence on the colour of the fired products. Clays with $Fe_2O_3$ content >5% would fire red while those with $Fe_2O_3$ content <5% would have brown to light brown colour (Murray, 2007). The threshold of <3% of $Fe_2O_3$ in the clay would potentially classify the samples as "light-firing" (M1) and "dark-firing" ceramic bodies (M2 and M3) (Dondi *et al.*, 2014). This was confirmed from the dominant wavenumber (Dc) and the purity of the colour (Pc) of the samples after firing at 1200°C (Table 2). The standard deviation values indicate that the samples do not have completely uniform colour

TABLE 2. Colour properties and semi-quantitative estimates of the goethite content.

| | Samples | | |
|---|---|---|---|
| % | M1 | M2 | M3 |
| Whiteness | 57.4 | 51.9 | 49.5 |
| Yellowness | 9.5 | 28.9 | 23.1 |
| Dc (nm) | 583.8(0.2) | 589.3(0.2) | 589.1(0.1) |
| Pc (%) | 15.6(0.6) | 37.1(1.1) | 30.4(1.1) |
| Goethite (%) | 3 | 9 | 10 |

https://doi.org/10.1180/claymin.2017.052.3.04 Published online by Cambridge University Press

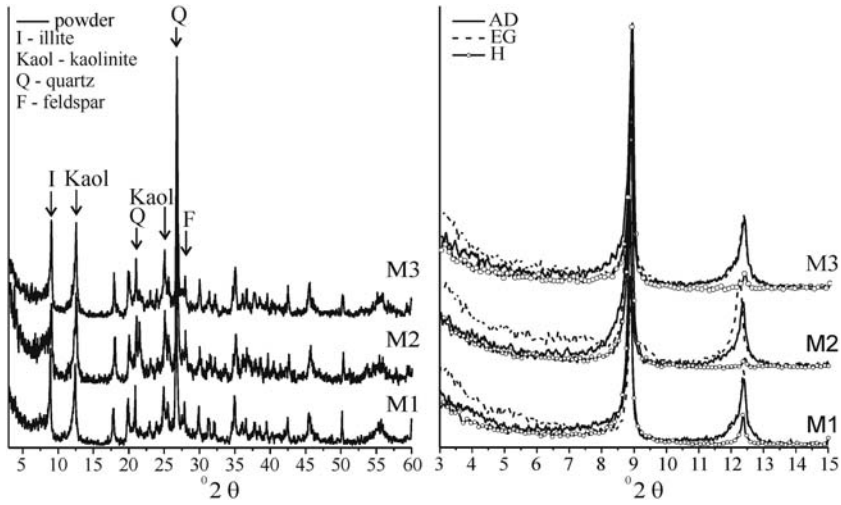


FIG. 4. XRD patterns of samples M1, M2 and M3 (AD – air dried, EG – saturated, H – heated). Left: bulk samples, right: clay fractions.

(Table 2) although surfaces were even and free of flaws or cracks. The colour of the M1 sample was lighter compared to its counterparts due to the low concentration of iron oxides.

The XRD patterns of bulk sediments and oriented clay fractions are shown in Fig. 4. The samples can be characterized as illite and kaolinite clay. Illite and kaolinite were identified by the reflections at 10 Å and 7.2 Å, respectively, which are not affected by ethylene-glycol solvation. The intensity of the kaolinite 001 reflections decreased after heating. Characteristic reflections for swelling minerals were not found after ethylene-glycol solvation. These results were very similar to those of M1 and M2 studied by Milošević *et al.* (2016). The presence of halloysite was not verified unambiguously. Identification of the dehydrated form of halloysite by XRD may be ambiguous because its 001 basal spacing at 7 Å is comparable to that of disordered kaolinite (Brindley, 1980). Quartz and feldspars were detected in the XRD patterns of the bulk powder samples. The XRD data for M1 and M2 were published previously (Milošević *et al.*, 2016). The main minerals identified in M3 were illite and kaolinite, quartz (Q) and feldspars (F).

The chemical composition of the clays is listed in Table 3. The $SiO_2$ varies from 49.86 to 53.21 wt.%, while $Al_2O_3$ content was between 24.54 and 33.60 wt.%. The considerable mass loss on ignition (LOI) associated with large $Al_2O_3$ and low $SiO_2$ contents might be associated with increasing contents of clay minerals (Boussen *et al.*, 2016; Milošević *et al.*, 2016).

TABLE 3. Chemical compositions of the clays.

| Oxides (wt.%) | M1 | M2 | M3 |
|---|---|---|---|
| $SiO_2$ | 49.86 | 53.21 | 52.53 |
| $Al_2O_3$ | 33.60 | 24.54 | 25.92 |
| $Fe_2O_3$ | 2.64 | 8.37 | 8.74 |
| $K_2O$ | 4.45 | 4.50 | 4.18 |
| $Na_2O$ | 0.12 | 0.04 | 0.13 |
| CaO | 0.29 | 0.22 | 0.35 |
| MgO | 1.13 | 0.65 | 1.12 |
| LOI | 7.50 | 8.07 | 6.10 |
| Total (wt.%) | 99.60 | 99.60 | 99.07 |

Analyses of M1 and M2 are from Milošević *et al.* (2016).

TABLE 4. Calculated semi-quantitative amounts of minerals in the samples investigated.

| Minerals (%) | M1 | M2 | M3 |
|---|---|---|---|
| Kaolinite | 24 | 20 | 22 |
| Illite | 48 | 46 | 46 |
| Quartz | 21 | 21 | 19 |
| Feldspars | 2 | 1 | 3 |
| Goethite | 3 | 9 | 10 |
| Impurities | 1 | 0 | 0 |

https://doi.org/10.1180/claymin.2017.052.3.04 Published online by Cambridge University Press

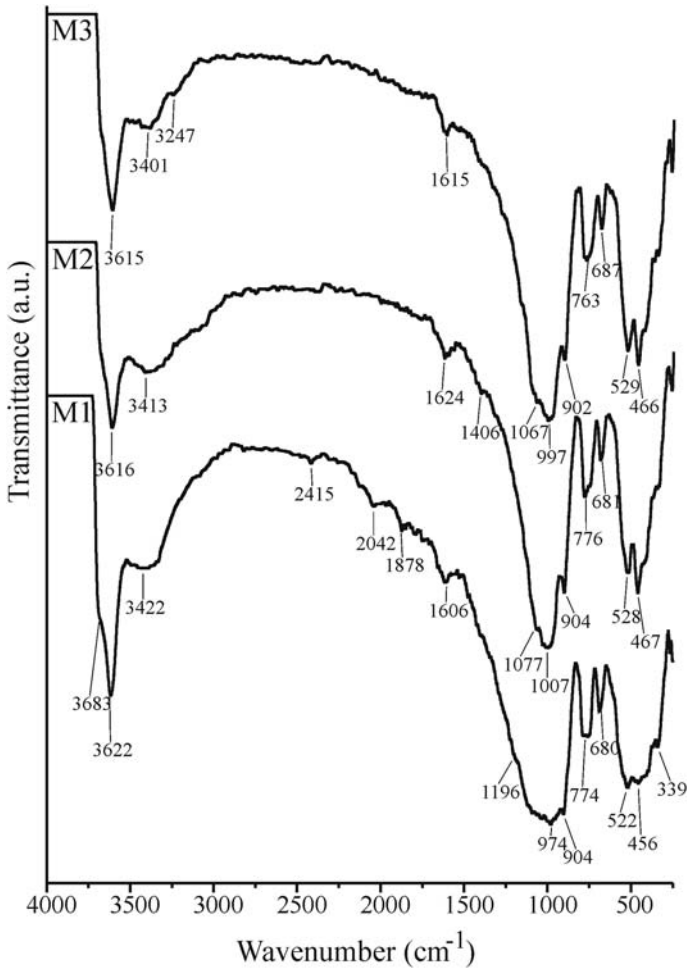


FIG. 5. IR spectra of samples M1, M2 and M3.

The low abundance of CaO samples indicates minor carbonate minerals.

The semi-quantitative estimates of the mineral phases present in samples M1, M2 (Milošević *et al.*, 2016) and M3, obtained from the XRD traces with Rietveld refinement and stoichiometric calculations, are listed in Table 4.

Stoichiometric calculations were based on the ideal formula unit a for a given mineral with semi-quantitative amounts of minerals established by Rietveld refinement. All iron was assigned to iron minerals, especially goethite, which was confirmed by DTA. Goethite is considered to have a disordered crystal structure because it was not detected by XRD. Potassium was mostly assessed as being present in illite and only a small percentage was combined with Na in feldspar. All samples contain Ca-rich plagioclase with 58–76% anorthitic component. In order to achieve a desired glassy phase for floor-tile composites it is necessary to have ~50–60% K-feldspar (Norton, 1970; Abadir *et al.*, 2002). The samples investigated contain less feldspar but have greater illite contents. Potassium derived from feldspar or illite is a necessary flux for the manufacture of porcelain. The quartz content was calculated from the excess $SiO_2$ which was not included in clay minerals and feldspars (Milošević *et al.*, 2016). Quartz has a high coefficient of thermal expansion which affects the strength of porcelain (Jackson & Mills, 2001; Kamseu *et al.*, 2007).

https://doi.org/10.1180/claymin.2017.052.3.04 Published online by Cambridge University Press

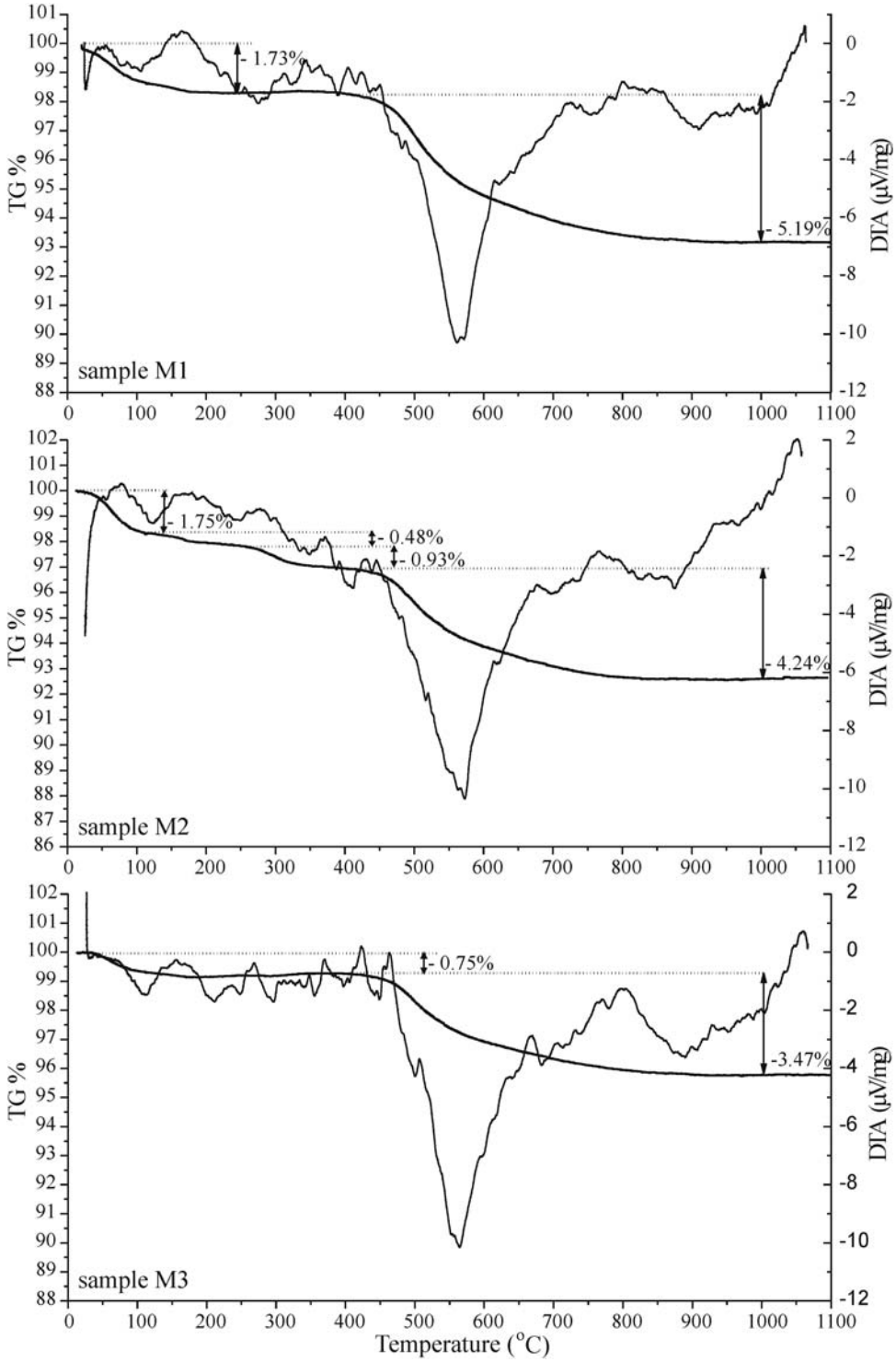


FIG. 6. DTA/TG curves of the clay samples.

https://doi.org/10.1180/claymin.2017.052.3.04 Published online by Cambridge University Press

The CEC of the samples varied between 6 and 7 meq/100 g while for samples of <2 μm, values were slightly higher, ~10 meq/100 g, typical of kaolin minerals (Grim, 1953). According to the Methylene Blue index, samples could be classified as low-plasticity kaolinitic loams (Chiappone *et al.*, 2004; Dondi *et al.*, 2014).

The IR spectra of samples M1, M2 and M3 are shown in Fig. 5. The presence of clay minerals was confirmed in all samples by the absorption bands between 3700 and 3620 $cm^{-1}$, assigned to stretching vibrations of the OH groups of clay minerals. The shoulder near 3683 $cm^{-1}$ represents kaolinite OH-stretching vibrations and the relative intensity of this band is indicative of the kaolinite abundance in the samples (Madejová *et al.*, 2002; Madejová, 2003; de Almeida Azzi *et al.*, 2016). According to the relative intensity of this band, the abundance of kaolinite decreases in the following order: M1 > M3 > M2, in agreement with the semi-quantitative estimations with XRD.

The bands in the region between 1196 and 974 $cm^{-1}$ are attributed to Si–O stretching vibrations while those near 520 and 460 $cm^{-1}$ correspond to Si–O–Al and Si–O–Si bending vibrations, respectively. The small shoulder at 1406 $cm^{-1}$ indicates the presence of minor carbonate minerals (M2). The quartz doublet is less pronounced but has a greater intensity at ~775 $cm^{-1}$ indicating a significant amount of quartz minerals in agreement with the semi-quantitative XRD results. Bands assigned to feldspars are observed at ~680 $cm^{-1}$.

The DTA-TG curves of clay samples are presented in Fig. 6. The DTA curves exhibit four endothermic events. The first, at ~120°C, with mass loss of 1.5–2.5%, is attributed to the removal of the adsorbed water in the clay minerals (Bradley & Grim, 1951). The endothermic peaks between 300 and 450°C (mass loss ~0.5%), are attributed to the presence of goethite and organic matter. The main endothermic event, with a maximum at ~560°C and mass loss of ~4%, was caused by dehydroxylation of kaolin minerals and illite (Brown & Brindley, 1984; Jouenne, 1990; Boussen *et al.*, 2016). The endothermic event at ~900°C indicates the collapse of the illite lattice and formation of spinel (Gaudette *et al.*, 1964; Földvári, 2011) without significant mass loss. The band at ~1050°C corresponds to the formation of mullite which forms from kaolinite and illite at temperatures of >1000°C (Okada & Otsuka, 1986; Gonzalez-Garcia *et al.*, 1990; Aras, 2004). The TG curves show a total mass loss at 1000°C of 6.83, 7.39 and 4.22 wt.% for M1, M2 and M3, respectively.

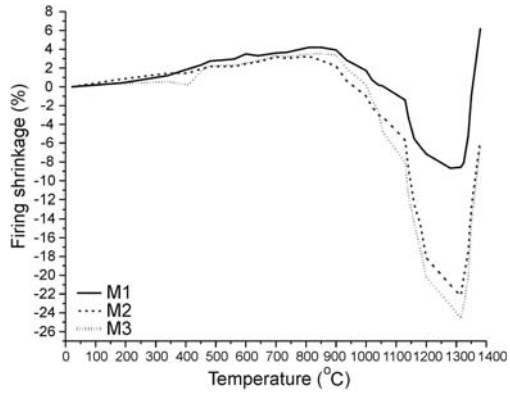


FIG. 7. Shrinkage after firing in the temperature range 20–1400°C.

The firing shrinkage curves of the three samples investigated are shown in Fig. 7. In general the curves show a small degree of shrinkage at ~400°C followed by a plateau caused by expansion and deformation of the ceramic bodies. Shrinkage at 400°C was a consequence of dehydroxylation of goethite and combustion of organic matter. The smaller expansion at ~570°C is attributed to the α–β quartz transition (Cruz *et al.*, 2015) and is expected due to the relatively large quartz content in the samples.

The shrinkage between 870°C and 1120°C is attributed to the lattice collapse of illite and the intial formation of the mullite phase (Cruz *et al.*, 2015). At ~1100°C, the rate of shrinkage increases indicating the beginning of sintering. The sintering process was terminated at 1250–1300°C. At higher temperatures the viscosity of the liquid phase decreases and the ceramic body deforms. The larger shrinkage observed in M2 and M3 compared to the M1 is attributed to the goethite content in the samples. The transformation of goethite to hematite was followed by a considerable decrease in volume producing additional porosity. During sintering, closure of the pores led to densification of the body. Therefore, for the same density the greater shrinkage should be linked with the greater porosity. The firing curves suggest that the firing temperature during manufacture should be between 900 and 1100°C, depending on the firing regime.

The plasticity values of the studied samples are shown in Table 5. According to their PI values (PI 10–15%) the samples have low plasticity (L.C.P.C., 1987). The LL varies between 33 and 42%, in agreement with the range defined in the literature (30–60%) for compositions used in ceramics (L.C.P.C., 1987;

https://doi.org/10.1180/claymin.2017.052.3.04 Published online by Cambridge University Press

TABLE 5. Plasticity values of samples studied (wt.%).

| Sample | LL | PL | PI |
|---|---|---|---|
| M1 | 36 | 23 | 13 (0.1) |
| M2 | 42 | 28 | 14 (0.7) |
| M3 | 33 | 20 | 12 (0.5) |

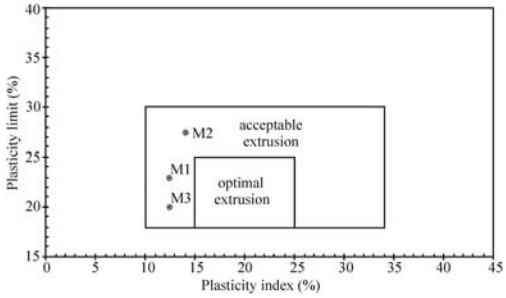


FIG. 8. Extrusion behaviour of the samples examined.

Baccour *et al.*, 2009). High PL values might indicate possible difficulties in the drying process, although they might contribute to reduction of wear during extrusion (Monteiro & Vieira, 2004). In extrusion processes, the PI values should exceed 10% (Abajo 2000; Vieira *et al.*, 2008). The plasticity of the clays investigated is acceptable for extrusion (Fig. 8, Abajo, 2000).

## CONCLUSION

The clay samples from the Miličinica deposit (Valjevo, SW Serbia) consist mainly of kaolinite, illite, quartz, goethite and smaller amounts of feldspars. The greatest clay mineral content (kaolinite and illite) and the smallest amount of goethite were observed in sample M1. The average grain size of the <2 μm clay fraction was ~0.7 μm and the CEC ranges between 6 and 7 meq/100 g. From a technological point of view, the clay samples studied were characterized as low-plasticity, kaolinitic loams which are generally suitable for a wide range of ceramic industries. All the samples studied have PL values >10% which makes them suitable for extrusion processes. The materials are suitable for vertically perforated bricks (M1 and M2 samples) and hollow products (M3). The greater goethite content in M2 and M3 samples (>9 wt.%) limits their application in the ceramic industry but possible reduction might be achieved by leaching with organic acids. Such an investigation has yet to be carried out.

## ACKNOWLEDGEMENTS

The present study was supported by the Ministry of Education and Science, Republic of Serbia, Project no. 176010.

## REFERENCES

Abadir M.F., Sallam E.H. & Bakr I.M. (2002) Preparation of porcelain tiles from Egyptian raw materials. *Ceramics International*, **28**, 303–310.

Abajo M.F. (2000) Manual sobre Fabricación de Baldosas, Tejas y Ladrillos. Eds. Beralmar S.A., Barcelona, Columbia, 360 pp.

AFNOR NF EN ISO 10693 (1995) *Soil Quality. Determination of Carbonate Content. Volumetric Method*. International Standard Organization, Geneva, Switzerland.

Aras A. (2004) The change of phase composition in kaolinite- and illite-rich clay-based ceramic bodies. *Applied Clay Science*, **24**, 257–269.

ASTM (1984) Standard test method for methylene blue index of clay (C 837-99). *1984 Annual Book of ASTM Standards*, sect. 15, vol. **15.02**. American Society for Testing and Materials (ASTM), Philadelphia, Pennsylvania, USA.

Atterberg A. (1911) Die Plastizität der Tone. *Internationale Mitteilungen der Bodenkunde*, **1**, 4–37.

Baccour H., Medhioub M., Jamoussi F. & Mhiri T. (2009) Influence of firing temperature on the ceramic properties of Triassic clays from Tunisia. *Journal of Materials Processing Technology*, **209**, 2812–2817.

Boussen S., Sghaier D., Chaabani F., Jamoussi B. & Bennour A. (2016) Characteristics and industrial application of the Lower Cretaceous clay deposits (Bouhedma Formation), Southeast Tunisia: Potential use for the manufacturing of ceramic tiles and bricks. *Applied Clay Science*, **123**, 210–221.

Bradley W.F. & Grim R.E. (1951) High temperature thermal effects of clay and related materials. *American Mineralogist*, **36**, 182–201.

Brindley G.W. (1980) Order-disorder in the clay mineral structures. Pp. 125–196 in: *Crystal Structures of Clay Minerals and Their X-ray Identification* (G.W. Brindley & G. Brown, editors). Mineralogical Society, London, 495 pp.

Brown G. & Brindley G.W. (1984) *Crystal Structures of Clay Minerals and Their X-ray Identification*. Mineralogical Society, London, 495 pp.

Bundy W.M. & Ishley J.N. (1991) Kaolin in paper filling and coating. *Applied Clay Science*, **5**, 397–420.

https://doi.org/10.1180/claymin.2017.052.3.04 Published online by Cambridge University Press

Burst J.F. (1991) The application of clay minerals in ceramics. *Applied Clay Science*, **5**, 421–443.

Carretero M.I. & Pozo M. (2009) Clay and non-clay minerals in the pharmaceutical industry. Part I. Excipients and medical applications. *Applied Clay Science*, **46**, 73–80.

Chiappone A., Marello S., Scavia C. & Setti M. (2004) Clay mineral characterization through the methylene blue test: comparison with other experimental techniques and applications of the method. *Canadian Geotechnical Journal*, **41**, 1168–1178.

CIE (1932) 1931 Commission Internationale de l'Eclairage Proceedings. Huitième session. Cambridge University Press, Cambridge, UK, pp. 19–29.

Cruz R.C.D., Perottoni C.A., Zorzi J.E. & Emiliano J.V. (2015) Technological characterization of heavy clay from the Caí River Valley in Brazil. *Interceram*, **64**, 14–19.

de Almeida Azzi A., Osacký M., Uhlík P., Čaplovičová M., Zanardo A. & Madejová J. (2016) Characterization of clays from the Corumbataí formation used as raw material for ceramic industry in the Santa Gertrudes district, São Paulo, Brazil. *Applied Clay Science*, **132–133**, 232–242.

DIN ISO 11277, Deutsches Institut für Normung (2002) *Bodenbeschaffenheit – Bestimmung der Partikelgr ßenverteilung in Mineralb den*. Beuth, Berlin.

Dondi M., Fabbri B. & Guarini G. (1998) Grain-size distribution of Italian raw materials for building clay products: a reappraisal of the Winkler diagram. *Clay Minerals*, **33**, 435–442.

Dondi M., Raimondo M. & Zanelli C. (2014) Clays and bodies for ceramic tiles: Reappraisal and technological classification. *Applied Clay Science*, **96**, 91–109.

Felhi M., Tlili A., Gaied M.E. & Montacer M. (2008) Mineralogical study of kaolinitic clays from Sidi El Bader in the far north of Tunisia. *Applied Clay Science*, **39**, 208–217.

Filipović I., Gagić N., Rodin V. & Avramović V. (1973) Tumač za list Vladimirci L. Pp. 34–124 in: *Zavod za Geološka i Geofizička Istraživanja* (M. Dimitrijević, S. Karamata, B. Sikošek & D. Veselinović, editors). Privredni Pregled, Beograd, Maršala Birjuzova 3, 58 pp.

Földvári M. (2011) Handbook of thermogravimetric system of minerals and its use in geological practice. *Occasional Papers of the Geological Institute of Hungary*, vol. **213** (G. Maros, editor). Geological Institute of Hungary, 180 pp.

Frost R.L., Van Der Gaast S.J., Zbik M., Kloprogge J.T. & Paroz G.N. (2002) Birdwood kaolinite: a highly ordered kaolinite that is difficult to intercalate – an XRD, SEM and Raman spectroscopic study. *Applied Clay Science*, **20**, 177–187.

Gaudette H.E., Eades J.L. & Grim R.E. (1964) The nature of illite. *Clays and Clay Minerals*, **13**, 33–48.

Gonzalez-Garcia F., Romero-Acosta V., Garcia-Ramos G. & Gonzalez-Rodriguez M. (1990) Firing transformations of mixtures of clays containing illite, kaolinite and calcium carbonate used by ornamental tile industries. *Applied Clay Science*, **5**, 361–375.

Grim R.E. (1953) *Clay Mineralogy*. McGraw-Hill, New York, 384 pp.

Grim R.E. (1962) *Applied Clay Mineralogy*. McGraw-Hill, New York, 422 pp.

Grimshaw R.W. (1971) *Physics and Chemistry of Clay*. 4th Edition. Ernest Benn, London, 1024 pp.

Güven N. (2001) Mica structure and fibrous growth of illite. *Clays and Clay Minerals*, **49**, 189–196.

Harvey C.C. & Murray H.H. (1997) Industrial clays in the 21st century: A perspective of exploration, technology and utilization. *Applied Clay Science*, **11**, 285–310.

Jackson M.J. & Mills B. (2001) Vitrification heat treatment and dissolution of quartz grinding wheel bonding systems. *British Ceramic Transactions*, **100**, 1–8.

Jouenne C.A. (1990) *Traite de ceramiques et materiaux mineraux*. Editor: Septima, Paris, 657 pp.

Joussein E., Petit S., Churchman J., Theng B., Righi D. & Delvaux B. (2005) Halloysite clay minerals – a review. *Clay Minerals*, **40**, 383–426.

Kamseu E., Leonelli C., Boccaccini D.N., Veronesi P., Miselli P., Pellacani G. & Chinje Melo U. (2007) Characterisation of porcelain compositions using two china clays from Cameroon. *Ceramics International*, **33**, 851–857.

Lawrence W.G. (1972) *Ceramic Science for the Potter*. Chilton Book Co., Philadelphia, Pennsylvania, USA, 239 pp.

L.C.P.C. (1987) Limites d'Atterberg, limite de liquidité, limite de plasticité, method d'essai LPC, n°19. Publication L. C. P. C., 26 pp.

Madejová J. (2003) FTIR techniques in clay mineral studies. Review. *Vibrational Spectroscopy*, **31**, 1–10.

Madejová J., Kečkéš J., Pálková H. & Komadel P. (2002) Identification of components in smectite/kaolinite mixtures. *Clay Minerals*, **37**, 377–388.

Matthew G.O. & Fatile B.O. (2014) Characterization of vitrified porcelain tiles using feldspar from three selected deposits in Nigeria. *Research Journal of Recent Sciences*, **3**, 67–72.

Milošević M., Logar M., Dojčinović B., Rosić A. & Erić S. (2016) Diffuse reflectance spectra of methylene blue adsorbed on different types of clay samples. *Clay Minerals*, **5**, 1–15.

Mitrović A.A., Komljenović M.M. & Ilić B.R. (2009) Ispitivanja Mogućnosti Korišćenja Domaćih Kaolinskih Glina Za Proizvodnju Metakaolina. *Hemijska Industrija*, **63**, 107–113.

Monteiro S.N. & Vieira C.M.F. (2004) Influence of firing temperature on the ceramic properties of clays from Campos dos Goytacazes, Brazil. *Applied Clay Science*, **27**, 229–234.

Mukherjee S. (2013) *The Science of Clays*. Applications in Industry, Engineering and Environment. Co-

https://doi.org/10.1180/claymin.2017.052.3.04 Published online by Cambridge University Press

published by Springer, The Netherlands with Capital Publishing Company, New Delhi, India, 335 pp.

Murray H.H. (1991) Overview – clay mineral applications. *Applied Clay Science*, **5**, 379–395.

Murray H.H. (1995) Applied clay mineralogy today and tomorrow. *Clay Minerals*, **34**, 39–49.

Murray H.H. (2007) *Applied Clay Mineralogy: Occurrences, Processing, and Application of Kaolins, Bentonites, Palygorskite-Sepiolite, and Common Clays*. Elsevier, Amsterdam, 180 pp.

Murray H.H. & Kogel J.E. (2005) Engineered clay products for the paper industry. *Applied Clay Science*, **29**, 199–206.

Norton F.H. (1970) *Fine Ceramics Technology and Applications*. McGraw-Hill Book Company, New York, 507 pp.

Okada K. & Otsuka N. (1986) Characterization of spinel phase from $SiO_2$–$Al_2O_3$ xerogels and the formation process of mullite. *Journal of the American Ceramic Society*, **69**, 652–656.

Prasad M.S., Reid K.J. & Murray H.H. (1991) Kaolin: processing, properties and applications. *Applied Clay Science*, **6**, 87–119.

Radosavljević S., Stojanović M. & Branković A. (1994) Ceramic clays of Tamnava Tertiary basin (west Serbia). *Industrial Ceramics*, **14**, 155–158.

Radosavljević S., Stojanović J., Radosavljević-Mihajlović A., Vuković N., Matijašević S., Stojanović M. & Kašić V. (2014) Ceramic clays from the western part of the Tamnava Tertiary Basin, Serbia: deposits and clay types. *Geoloski Anali Balkanskog poluostrva*, **75**, 75–83.

Rivi A. & Ries B. (1997) Single-line dry grinding technology. *Ceramic World*, **24**, 132–141.

Saikia N.J., Bharali D.J., Sengupta P., Bordoloi D., Goswamee R.L., Saikia P.C. & Borthakur P.C. (2003) Characterization, beneficiation and utilization of a kaolinite clay from Assam, India. *Applied Clay Science*, **24**, 93–103.

Silva-Valenzuela M.G., Matos C.M., Shah L.A., Carvalho F.M.S., Sayeg I.J. & Valenzuela-Diaz F.R. (2013) Engineering properties of kaolinitic clay with potential use in drugs and cosmetics. *International Journal of Modern Engineering Research (IJMER)*, **3**, 163–165.

Singh B. & Gilkes R.J. (1992) An electron optical investigation of the alteration of kaolinite to halloysite. *Clays and Clay Minerals*, **40**, 212–229.

Valášková M. (2015) Clays, clay minerals and cordierite ceramics – A review. *Ceramics – Silikáty*, **59**, 331–340.

Vieira C.M.F., Sánchez R. & Monteiro S.N. (2008) Characteristics of clays and properties of building ceramics in the state of Rio de Janeiro, Brazil. *Construction and Building Materials*, **22**, 781–787.

Viseras C., Aguzzi C., Cerezo P. & Lopez-Galindo A. (2007) Uses of clay minerals in semisolid health care and therapeutic products. *Applied Clay Science*, **36**, 37–50.

Wilson I.R. (1998) The constitution, evaluation and ceramic properties of ball clays. *Cerâmica*, **44**, 88–117.

Winkler H.G.F. (1954) Bedeutung der Korngrössenverteilung und des Mineral-bestandes von Tonen für die Herstellung grobkerarnischer Erzeugnisse. *Berichte der Deutschen Keramischen Gesellschaft*, **31**, 337–343.